Helmholtz-Zentrum Dresden-Rossendorf (HZDR)

HZDR
HELMHOLTZ ZENTRUM
DRESDEN ROSSENDORF

In situ measurements of non-equilibrium positron state defects during He irradiation in Si

Auguste, R.; Liedke, M. O.; Butterling, M.; Uberuaga, B. P.; Selim, F. A.; Wagner, A.; Hosemann, P.;

Originally published:

May 2023

Journal of Applied Physics 133(2023)18

DOI: https://doi.org/10.1063/5.0144308

Perma-Link to Publication Repository of HZDR:

https://www.hzdr.de/publications/Publ-35201

Release of the secondary publication
on the basis of the German Copyright Law § 38 Section 4.

In situ Measurements of non-equilibrium defects during He irradiation in Si

R. Auguste,[1] M. O. Liedke [2], M. Butterling [2], B.P. Uberuaga [3], F. A. Selim, [4,5] A. Wagner,[2] and P. Hosemann[6]*

[1] Department of Nuclear Engineering, University of California at Berkeley, Berkeley, USA

[2] Institute of Radiation Physics, Helmholtz-Zentrum Dresden-Rossendorf, Bautzner Landstr. 400, 01328 Dresden, Germany.

[3] Materials Science and Technology Division, Los Alamos National Laboratory, Los Alamos, New Mexico, CA, USA

[4] Center for Photochemical Sciences, Bowling Green State University, Bowling Green, Ohio, USA.

[5] Department of Physics and Astronomy, Bowling Green State University, Bowling Green, Ohio, USA.

[6] Lawrence Berkeley National Laboratory, Material Science Division, Berkeley, California, USA

*Corresponding author

Graphical Abstract:

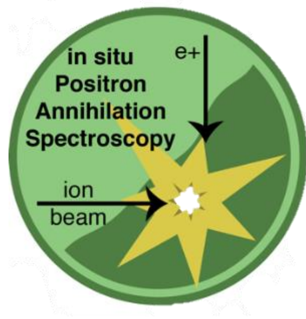

Abstract:

Radiation-induced property changes in materials originate with the energy transfer from an incoming particle to a lattice and the displacement of the atoms from their original location. The displaced atoms can, depending on conditions, lead to the formation of extended defects such as dislocation loops, voids, or precipitates. The non-equilibrium defects created during damage

events and that determine the extent of these larger defects are a function of dose rate, material, and temperature. However, these defects are transient and can only be probed indirectly. This work presents direct experimental measurements and evidence of non-equilibrium vacancy formation during irradiation, where in-situ positron annihilation spectroscopy was used to prove the generation of non-equilibrium defects in silicon.

Introduction

Radiation damage in materials can lead to physical and chemical property changes that degrade the properties of components and therefore limit their performance and lifetime. The energy transfer from the incoming radiation to the host atoms creates non-equilibrium defects. The evolution of these defects can, depending on conditions, lead to the failure of the material, for instance by the formation of extended defects. The buildup of extended defects is governed by how the initial point defects interact with each other and with pre-existing microstructural features such as grain boundaries or dislocations over time. As such, radiation damage is a truly multiscale in space and time, from atomic-sized point defects formed in femtoseconds to degradation of entire reactor pressure vessels over decades. The consequences of radiation effects manifest themselves in phenomena such as swelling, hardening, and embrittlement that occur on the macroscopic scale but the underlying physics is based on time and length scale relevant features within the material that are incredibly difficult to probe directly [1].

There are a large number of transient displacements in the radiation cascade, but most self-anneal within a time scale on the order of picoseconds [1,2], leaving just a relatively small number of defects. Conventional rate theory suggests there may be a steady-state concentration of defects generated during irradiation. [3] Mobile Frenkel pairs (vacancies and interstitials) formed throughout the solid during irradiation randomly move until they cease to exist either by recombination with the opposite type of defect or by incorporation into the lattice at fixed, sinks such as dislocations, grain boundaries, and voids. [3] While these remaining non-equilibrium defects can be characterized by probes such as XRD and TEM [4], so capturing the transient, small point defects that drive their evolution must be done in-situ, before they anneal out or aggregate into larger, extended, more stable defects.

The small size and non-equilibrium nature of the transient point defects makes a direct observation difficult. Instead, measurement tools have focused on observing larger defects or measure the effects of radiation indirectly by sampling other properties. Differential dilatometry [5], electrical resistivity measurements [6], or short, intense ion beam pulses [7] have been used to study these displacement cascades and the resulting atomic displacement damage. Further, stable defects such as displacement loops, voids, cavities larger than 1-2 nanometers can be observed with TEM studies or various diffraction techniques [8,9,10]. Larger stable extended defects in materials

created by irradiation present a multiscale problem with defect lifetimes ranging from picoseconds to years [11,12].

Studies observe and quantify these extended effects of radiation damage, but do not provide direct insight into the transient defects which drive the development of those extended effects. The survival of defects is a dynamic problem, so experimental verification of either the displacement damage or its evolution has proven to be difficult. In-situ techniques must be employed to experimentally quantify and verify the evolution of the damage cascade.

Positrons are a nondestructive analytical probe used to study point defects in nearly all material classes. Positron annihilation spectroscopy (PAS) introduces positrons (antiparticles of electrons) to a material, where they thermalize, diffuse, and eventually annihilate with electrons. [13] In the presence of defects, Doppler broadening positron annihilation spectroscopy (DB-VEPAS) studies the electron momentum distribution around the defect site while positron annihilation lifetime spectroscopy (PALS) studies the lifetime of the trapped positrons. Positrons have been used for many years to study radiation damage in materials, albeit almost exclusively postmortem [14]

In DB-VEPAS, the S-parameter, which corresponds to the annihilation fraction with low electron momentum valence electrons and open-volume defects are correlated allowing one to observe relative changes in the density of defects. The W-parameter represents the annihilation fraction with high momentum core electrons and can be utilized to reveal elemental decoration of the annihilation site by performing coincident DB-VEPAS [15]. Previous in-situ experiments have attempted DB-VEPAS [16, 17] using low energy slow positrons with low penetration depth into irradiated samples [18, 19]. These studies did not implant monoenergetic positrons leading to limiting depth resolution. In contrast, variable energy positron annihilation spectroscopy (VEPAS) allows for depth-resolved measurements of vacancy-type defects in a material with a continuous or pulsed, monoenergetic positron beam. Details of the calculations of positron implantation depth, distribution of defects, and analysis of defect component lifetimes can be found in the Supplementary Information (SI).

While experimental facilities with monoenergetic positron beams are limited, previous studies have demonstrated the usefulness of ex-situ VEPAS for studying surviving vacancy-type defects in ion-implanted and irradiated materials [20]. In this work, non-equilibrium defects were studied using *in-situ* VEPAS during ion irradiation featuring 5 keV He^+ in Si.

Methods

The commercially available n-type Si wafer was obtained. Silicon was chosen because its' defect dynamics at low doses are well-studied, especially with positrons, mostly due to prolific use of ion implantation in the semiconductor industry. In addition, silicon wafers provide readily available defect free substrates for investigating contrasts with ion-induced defects.

VEPAS measurements were performed at the positron facility in the Helmholtz-Zentrum Dresden-Rossendorf (HZDR) in Dresden, Germany. Doppler broadening VEPAS (DB-VEPAS) measurements were conducted at the apparatus for in-situ defect analysis (AIDA) [16] of the slow positron beamline (SPONSOR) [21]. Positrons were implanted into each sample with discrete kinetic energies E_p in the range between 0.05 and 10 keV, which allows for depth profiling from the surface down to about 650 nm. Before performing any experiments with the ion beam, a characterization of the bulk Si was done with VEPAS. These results were compared after the beam cycling experiment and subsequent sample exposure to oxidation to characterize overall changes in sample structure during the experiment.

In-situ measurement

The He^+ ion gun used for room-temperature irradiation was a Kaufman type with defocused beam area to about 5 mm in diameter and the ion current up to 1 mA. The highest ion implantation energy available was used, 5 keV, in order to drive the ions as deep into the sample as possible as to minimize surface contributions. The positron implantation energy was chosen to be at the maximum of the ion implantation depth. Unfortunately, as of today no higher energy ion source is available at the positron facility.

In order to measure the non-equilibrium vacancy defect survival, VEPAS was performed before and during ion irradiation for 30-minute intervals at room-temperature. This irradiation-measurement iteration pattern was performed 3 times to allow for relaxation of non-equilibrium defects. The objective was to observe how the open-volume defects from radiation damage change the S-parameter during and after ion irradiation.

For Si, depth-resolved positron measurements were taken for 30-minute intervals at E_p=2.45keV (about 200kcnts at 511 keV peak) before (b_i) and during (d_i) irradiation, where, i, is the irradiation iteration step. The ion implantation was 5 keV He^+ with I_{ion}=100 nA. After the last irradiation, a DB-VEPAS measurement was taken at E_p=2.45 keV, labeled "after" (a).

Ideally, all implanted positrons would sample defects created by incoming ions, so both the ion and positron implantation profiles were simulated to find maximum overlap. The ion implantation depth profile was simulated using SRIM Monte Carlo [22]. The beam fluence to damage conversion is based on SRIM Monte Carlo code simulations using the K-P mode with a displacement threshold energy of 40 eV for Si. The Mahkov positron implantation profile was simulated for positron energies (E_p) from 2.45 keV in Si. Figure 1 shows the overlapped ion and positron implantation profiles. Maximum overlap between positron implantation and ion damage was calculated at $E_p \approx 3$ keV, so $E_p = 2.45$ keV was chosen for the in-situ measurements.

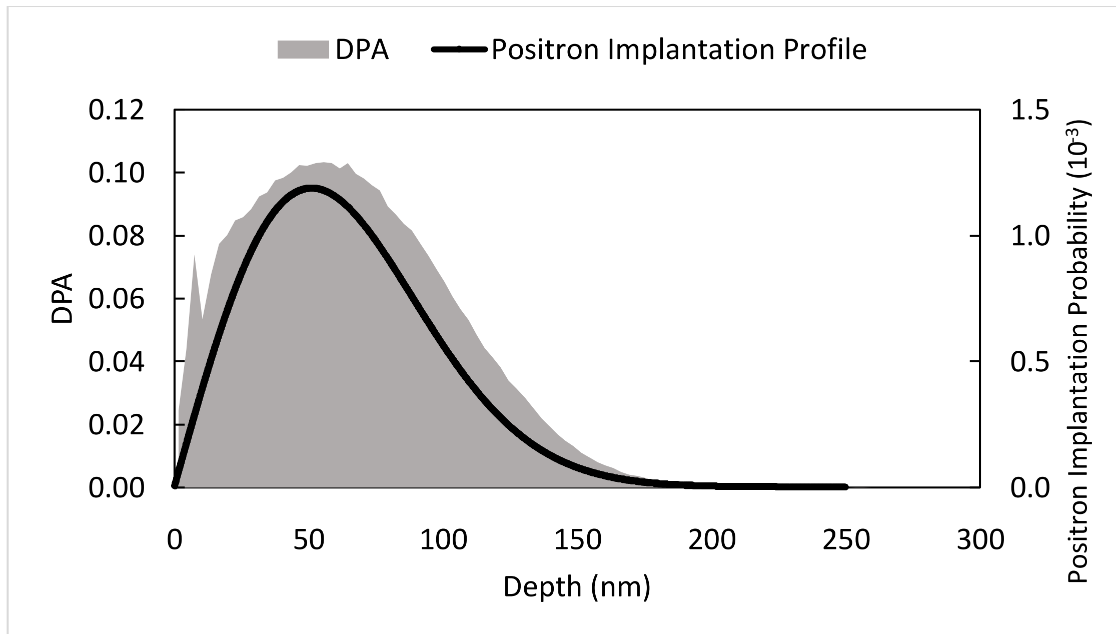

Fig. 1: Ion implantation damage profile calculated from SRIM (shaded in gray) and positron implantation profile at 2.45 keV (black). The He^+ implantation peak is slightly ahead of the dpa curve. The maximum overlap between positron implantation and ion damage was found at E_p = 2.45 keV, which determined the positron energy for the in-situ measurements.

After in-situ DB-VEPAS, variable energy positron annihilation lifetime spectroscopy (PALS) measurements were conducted on two Si samples at the mono-energetic positron source (MePS) beamline at HZDR, Germany [17, 23]: one pristine and the post-irradiation Si sample. Positrons were implanted into each sample with discrete kinetic energies E_p in the range between 0.05 and 12 keV, which allows for depth profiling from the surface down to about 850 nm. Details of the calculations of positron implantation depth and PALS analysis of defect lifetimes can be found in the Supplementary Information.

Results and Discussion

DB-PAS measurements were recorded during each irradiation iteration step with the ion beam either on or off. The results are shown in Figure 2, featuring S-parameters from each 30-minute DB-VEPAS acquisition at $E_p = 2.45$ keV (about 200kcnts at 511 keV peak) before (b_i) and during (d_i) irradiation. The relative increase of the S-parameter during irradiation steps suggests the development of defects. Furthermore, monovacancies have been found to be unstable (mobile) in Si at room temperatures, so the formation of more stable divacancies is likely. [24] The most important finding seen in Figure 2 is the increased S-parameter values during each irradiation step with the ion beam on (d_i) compared to the measurements before an irradiation step (b_i) with the ion beam off, which most likely probes a small fraction of non-equilibrium vacancies.

In addition to the increase in S-parameter after each irradiation, the difference in S-parameter between beam on/off seems to decrease with each iteration step, suggesting buildup of defects in the irradiated Si.

Despite apparent defect buildup, Si amorphization is not expected in this study because of the low dose delivered during irradiation. Dividing the beam current by the area gives an estimated dose per 30-minute irradiation of $9.8*10^{14}$ ions/cm^2. The total dose delivered to the sample is an order of magnitude less than the experimental threshold for Si amorphization at $8*10^{16}$ ions/cm^2 [25]. Amorphization can be limited because of recombination of point defects and surface annihilation from doses with light ions at low energies. [25, 26, 27] From SRIM, this incoming dose can be used to calculate overall dpa level. From each 30-minute irradiation, about 0.11 dpa is expected. Figure 2 shows the S-parameters of each irradiation step as a function of dpa delivered.

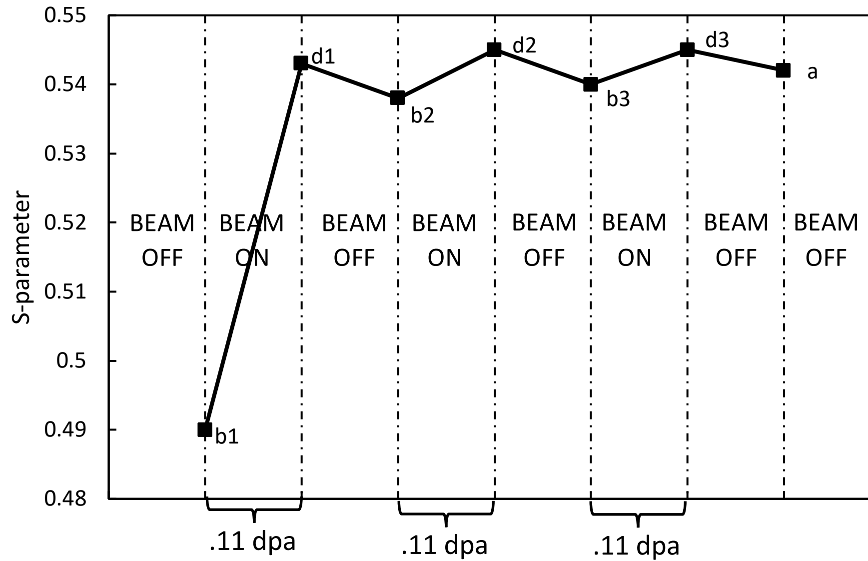

Fig. 2: S-parameters from 30-minute DBS VEPAS acquisition at E_p=2.45keV (about 200 kcnts at 511keV peak) before (b_i) and during (d_i), where, i, is the irradiation iteration step. For all irradiation steps, I_{ion}=100 nA. Errors are of the symbol size.

The DBS measurements at E_p = 2.45 keV sampled the peak ion damage from irradiation, but other damaged regions in the sample were assessed with VEPAS after the last irradiation iteration step i = 3. Figure 3[a] shows an increase in S-parameter after irradiation was seen at each positron energy from 0.5 – 10 keV. At the end of the beam cycling experiment, the vacuum chamber was vented to expose the sample to air at room temperature. The decrease in S-parameter after the sample is exposed to air is attributed to formation of an oxide layer on the surface, but the deeper damage still remains. The increased ortho-positronium (o-Ps) fraction after irradiation suggests surface oxide removal, which changes surface defect states and likely is responsible for the abrupt increase of S after first irradiation step (Figure. 3[b]) [28]. The near-surface SiO_2/Si region clearly changes with ion irradiation, even with light ions. TRIM calculations and acoustic impedance measurements [29] predict that this mechanism is due to defect formation and recoil of the native oxide atoms into the near surface silicon region. Future studies can explore deeper ion implantations in more detail with higher damage profiles away from the surface, removing surface effects. A follow-up study could, for example, use heavier implantation ions to create different defect types such as dislocation loops, larger vacancy clusters, and even amorphous irradiated regions in the crystalline substrate.

[a] [b]

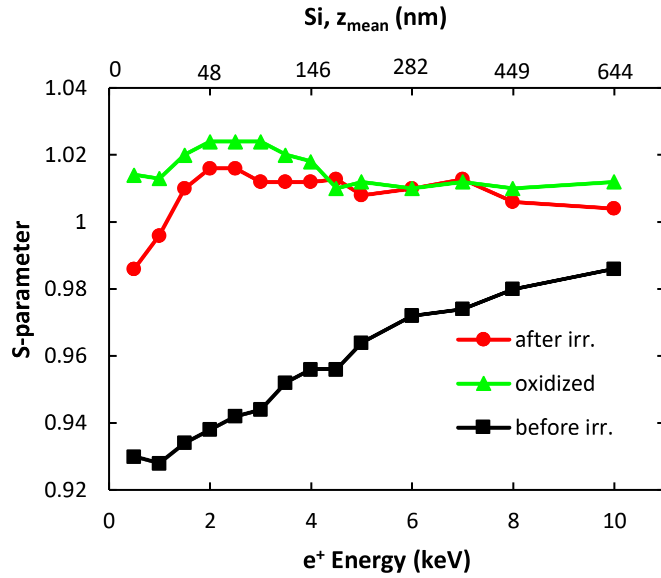

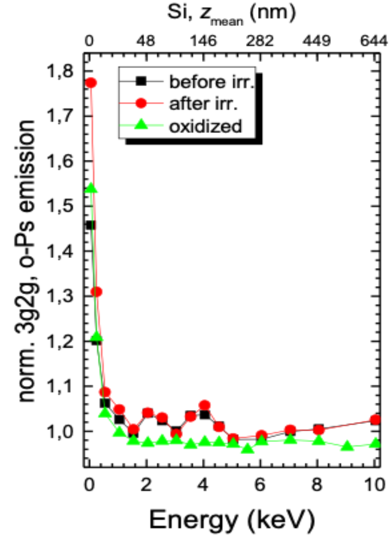

Fig. 3: [a] DB-VEPAS measurements before (black squares) irradiation and after the last irradiation iteration step i=3 (red circles), and after the sample exposition to air (green triangles). The measurements used a range of positron energies from 0.5 – 10 keV, and the expected depth from the sample surface sampled (z) is shown as well. Figure 3[b] shows the normalized 3g2g emission. Errors are of the symbol size.

Considering the existing DFT calculations (local-density approximation scheme with the Boronski and Nieminen enhancement) [32] of defect states in Si, a change of the S-parameter with respect to its bulk value (S_B) corresponding to a monovacancy is $S/S_B \approx 1.018$. For a divacancy, $S/S_B \approx 1.045$ is expected. The final in-situ S-parameter value after irradiation in the maximum damage region between 50 nm to 100 nm lays between these two defect states indicating that the maximum cluster size is a divacancy.

The size of vacancies has been also confirmed by ex-situ depth resolved positron annihilation lifetime spectroscopy (PALS) measurements. Details about the setup and measurements can be found in the SI. Figure 4 depicts PALS for the pristine and irradiated samples as a function of positron implantation energies. The upper x axis represents the positron mean implantation depth.

Figure 4 shows the first 20-30 nm region of the pristine sample is dominated by large vacancy clusters (>5 vacancies [7]), since only a single lifetime component is detected, $\tau_1 \approx 385$ ps ($I_1 \approx 99$ %). In the deeper parts of the sample, two lifetime components have been detected, where the first component τ_1 is less than the bulk lifetime in Si [31] and thus represents the reduced bulk lifetime, and the second component τ_2 represents a defect component. Despite surface effects, this strongly indicates the defect free existence of the initial state of Si. After irradiation, the first 100 nm is changed completely. The vacancy cluster size increases ($\tau_2 > 400$ ps; vacancy clustering), and a large number of most likely monovacancies (V_1 in Figure 4) is introduced $\tau_1 \approx 262$ ps [32]. The profiles of relative intensities resemble the ion damage profile, especially the τ_2 profile. Deeper in the irradiated sample, a signature of divacancies (V_2) or slightly larger defects is found. This divacancy signature found in PALS agrees directly with the DB-VEPAS results in which divacancies are also observed as the major defect fraction.

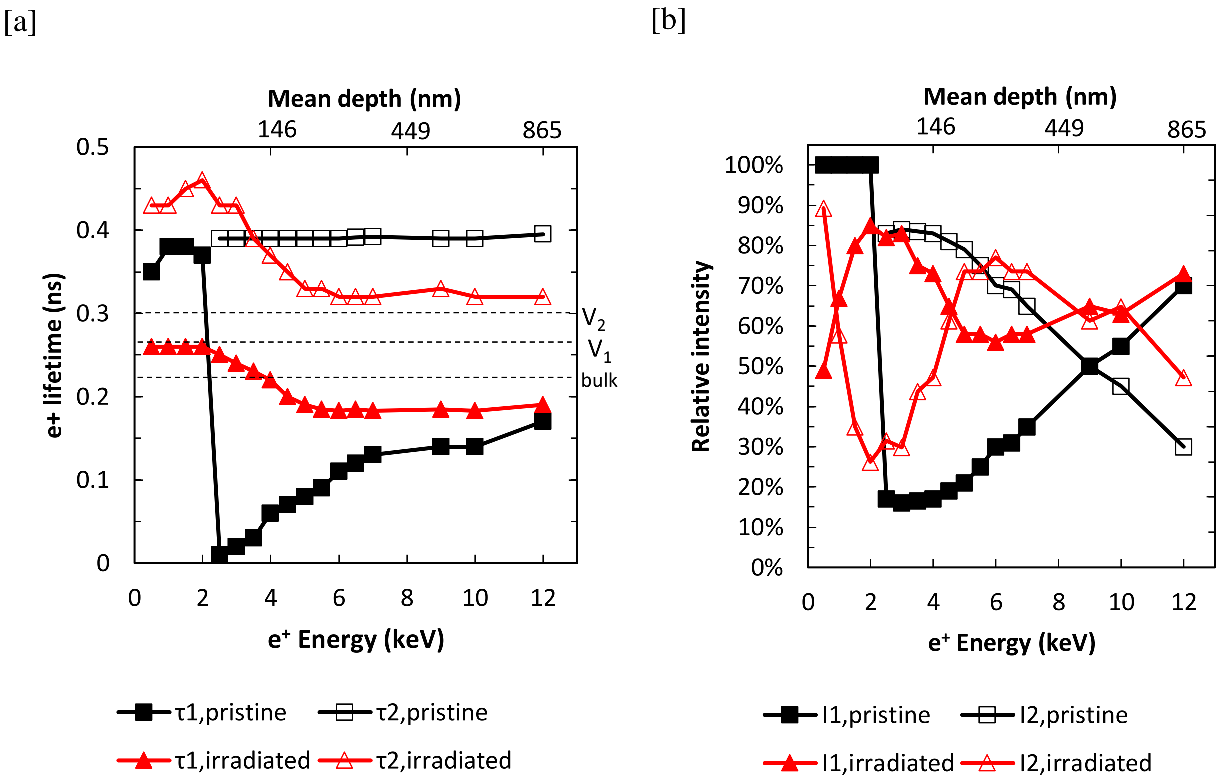

Figure 4: PALS analysis for pristine (closed symbols) and He^+ irradiated (open symbols) Si substrate. [a] The first τ_1 (squares) and the second τ_2 (circles) lifetime component as a function of

positron implantation energy and mean positron implantation depth, <z> as well as [b] the lifetime components' relative intensities I_1 and I_2, respectively. Errors are of the symbol size.

This study is limited to in-situ DBS as that is the only in-situ positron capability available today. It can only measure relative changes in defect concentration, as opposed to PALS, which can quantify absolute changes. Future experiments should investigate the changes in absolute non-equilibrium defect population under irradiation and annealing. In-situ investigations under extreme environments will promote understanding of non-equilibrium defect contribution to extended deformation effects of materials under corrosion, pressure, or stress.

The study was also limited by the range of ion implantation (peak range of approximately 50 nm) due to experimental limitations. Shallow ion implantations complicate analysis because of the surface effects that are present within 100 nm, especially the positron implantation distribution superimposed with at least partial back diffusion of positrons to the surface and the surface 2-3 nm oxide that complicates a detailed analysis. In the future, deeper ion implantations must be performed to combat the effect of diffusion and formation of positronium or other surface effects.

Conclusion

The effect of non-equilibrium defects from radiation damage in Si was investigated by in-situ depth-resolved DB-VEPAS measurements during ion irradiation. Cycling the ion beam on and off allowed for investigation of non-equilibrium defect populations during and after irradiation with positron spectroscopy. Significant increases in the defect population were observed as S-parameter values during irradiation (ion beam on) were higher compared to when the ion beam was off, which indicates the presence of non-equilibrium vacancies. The decreases in S-parameter after turning the ion beam off highlighted the importance of in-situ measurements for capturing relaxation of the non-equilibrium vacancies induced by irradiation. From the absolute S-parameter increase the defect states were determined to be a mixture of mono- and di-vacancies. Shallow ion implantation and DBS measurements limited this study to relative investigation of defect population, but in the future, in-situ PALS with irradiation could quantify true defect populations of non-equilibrium vacancies. Further in-situ studies are needed to understand the true defect concentration of materials during irradiation, as that will drive the materials' response in a number of contexts, including irradiation environments with added corrosion, pressure, or stress.

Supplementary Material

See supplementary material for positron implantation profile information, DB-VEPAS analysis, and post-irradiation PALS analysis details of the studied Si samples.

Acknowledgements

This work was supported as part of FUTURE (Fundamental Understanding of Transport Under Reactor Extremes), an Energy Frontier Research Center funded by the U.S. Department of Energy, Office of Science, Basic Energy Sciences. This work was supported by the U.S. Department of Energy through the Los Alamos National Laboratory. Los Alamos National Laboratory is operated by Triad National Security, LLC, for the National Nuclear Security Administration of U.S. Department of Energy (Contract No. 89233218CNA000001). Parts of this research were carried out at ELBE at the Helmholtz-Zentrum Dresden-Rossendorf (HZDR), a member of the Helmholtz Association. We would like to thank the facility staff for assistance (Ahmed G. Attallah and Eric Hirschmann). This work was partially supported by the Impulse-und Net-working fund of the Helmholtz Association (FKZ VH-VI-442 Memriox), and the Helmholtz Energy Materials Characterization Platform (03ET7015). This work was also supported by the Ron & Gail Gester Fellowship at the University of California, Berkeley.

References

1. Wirth, B. D., Caturla, M. J., De La Rubia, T. D., Khraishi, T., and Zbib, H., Nuclear Instruments and Methods in Physics Research Section B: Beam Interactions with Materials and Atoms 180.1-4, 23 (2001).
2. Robach, J. S., Robertson, I. M., Wirth, B. D., & Arsenlis, A., Philosophical Magazine, 83.8, 955 (2003).
3. Wiedersich, H. Radiation Effects 12.1-2, 111 (1972).
4. Stoller, R.E., Primary radiation damage formation, 1st ed. Ch. 1, Elsevier Ltd, Amsterdam, Netherlands, (2019)
5. Kerl, R., Wolff, J., & Hehenkamp T., Intermetallics 7, 301 (1999).
6. Dimitrov, C., M. Tenti, and O. Dimitrov. Journal of Physics F: Metal Physics 11.4, 753 (1981).

7. Persaud, A., Barnard, J.J., Guo, H., Hosemann, P., Lidia, S., Minor, A.M., Seidl, P.A. and Schenkel, T., Physics Procedia 66, 604 (2015).
8. Sprouster, D. J., Sun, C., Zhang, Y., Chodankar, S. N., Gan, J., & Ecker, L. E., Scientific Reports 9.1, 1 (2019).
9. Lupinacci, A., Chen, K., Li, Y., Kunz, M., Jiao, Z., Was, G.S., Abad, M.D., Minor, A.M. and Hosemann, P., Journal of Nuclear Materials 458, 70 (2015)
10. Yan, Q., Gigax, J., Chen, D., Garner, F. A., & Shao, L, Journal of Nuclear Materials 480, 420 (2016).
11. Wirth, B.D., Caturla, M.J., De La Rubia, T.D., Khraishi, T. and Zbib, H., Nuclear Instruments and Methods in Physics Research Section B: Beam Interactions with Materials and Atoms, 180.1-4, 23. (2001)
12. Robach, J.S., Robertson, I.M., Wirth, B.D. and Arsenlis, A., Philosophical Magazine, 83.8, 955 (2003).
13. Hautojärvi, P. *Positrons in Solids*, 1st ed., (Springer-Verlag, Berlin Germany 1979) pp.491-522.
14. Selim, F.A., Materials Characterization 174, 110952 (2021).
15. Clement, M., De Nijs, J.M.M., Balk, P., Schut, H. and Van Veen, A., Journal of Applied Physics 79, 9029 (1996).
16. Liedke, M.O., Anwand, W., Bali, R., Cornelius, S., Butterling, M., Trinh, T.T., Wagner, A., Salamon, S., Walecki, D., Smekhova, A. and Wende, H. Journal of Applied Physics, 117.16, 163908 (2015).
17. Wagner, A., Butterling, M., Liedke, M. O., Potzger, K. & Krause-Rehberg, R. Positron annihilation lifetime and Doppler broadening spectroscopy at the ELBE facility. in AIP Conference Proceedings 1970, 040003 (2018).
18. Kinomura, A., Suzuki, R., Ohdaira, T., Oshima, N., O'Rourke, B.E., and Nishijima, T., Physics Procedia 35, 111 (2012).
19. Kinomura, A., Suzuki, R., Ohdaira, T., Oshima, N., O'Rourke, B.E. and Nishijima, T., Journal of Physics: Conference Series 443.1, 012043 (2013).
20. Knights, A. P., Malik, F., and Coleman, P.G. Applied Physics Letters 75.4, 466 (1999).
21. Anwand, W., Brauer, G., Butterling, M., Kissener, H. R., & Wagner, A., Defect and Diffusion Forum 331, 25 (2012).

22. Ziegler, J.F., Ziegler, M.D. and Biersack, J.P., Nuclear Instruments and Methods in Physics Research Section B: Beam Interactions with Materials and Atoms, 268.11-12, 1818 (2010).
23. Wagner, A., Anwand, W., Attallah, A.G., Dornberg, G., Elsayed, M., Enke, D., Hussein, A.E.M., Krause-Rehberg, R., Liedke, M.O., Potzger, K. and Trinh, T.T. Journal of Physics: Conference Series 791.1, 012004 (2017).
24. Staab, T. E. M., Sieck, A., Haugk, M., Puska, M. J., Frauenheim, T., & Leipner, H. S., Physical Review B 65.11, 115210 (2002).
25. Morehead, F. F., Crowder, B. L., and Title R. S., Journal of Applied Physics 43.3, 1112 (1972).
26. Pelaz, L., Marqués, L. A., & Barbolla, J., Journal of Applied Physics 96.11, 5947 (2004).
27. Huang, X., Balooch, M., Xie, T., Leuber, S., Hosemann, P., Journal of Applied Physics (2022).
28. Coleman, P. G., Chilton, N. B. & Baker, Journal of Physics: Condensed Matter 2.47, 9355 (1990).
29. Gorham, C.S., Hattar, K., Cheaito, R., Duda, J.C., Gaskins, J.T., Beechem, T.E., Ihlefeld, J.F., Biedermann, L.B., Piekos, E.S., Medlin, D.L. and Hopkins, P.E., Physical Review B 90.2, 024301 (2014).
30. Hakala, M., Puska, M. J. & Nieminen, R. M. Physical Review B 57, 7621 (1998).
31. Mäkinen, S., Rajainmäki, H., & Linderoth, S., Physical Review B, 42.17, 11166 (1990).
32. Robles, J. C., Ogando, E., & Plazaola, F., Journal of Physics: Condensed Matter 19(17), 176222, (2007).

Supplementary Material

Positron Implantation Profile

The positron implantation profile is described by the exponential probability density function, P(z), in Equation 1 [1]:

$$P(z) = \frac{1}{\langle z \rangle} e^{-\frac{z}{\langle z \rangle}} \qquad (1)$$

where z is the depth from the sample surface. The mean penetration depth of positrons, $\langle z \rangle$, is given by the Makhov positron stopping expression as a function of positron implantation energy, E_p and using Equation 2 [1]:

$$\langle z \rangle = \frac{A}{\rho}(E_p)^n \quad (2)$$

where A = 3.6 ug/cm^2 keV$^{-1.6}$ and n = 1.6 are independent empirical parameters [2], and ρ is the material density which is considered here to be 2.3290 g/cm^3 for pure Si. This stopping profile does not take into account subsequent diffusion of positrons or formation of positronium. Positronium formation is expected at the surface for shallow ion irradiations and can be characterized using the 3g2g signal representing ortho-Positronium (o-Ps) formation. o-Ps is generated at surfaces of pores and at the film/vacuum interface. Epithermal and thermally excited positrons can reach the surface easier and contribute to the o-Ps emission in defect free crystals. [3] Unfortunately, the formation of positronium makes very shallow experiments difficult.

DB-VEPAS analysis

For DB-VEPAS data acquisition, thermalized positrons have very small momentum compared to the electrons upon annihilation, a broadening of the 511 keV line is observed mostly due to momentum of the electrons, which is measured with one or two high-purity Ge detectors (energy resolution of 1.09 ± 0.01 keV at 511 keV). This broadening is characterized by two distinct parameters S and W defined as a fraction of the annihilation line in the middle (511 ± 0.70 keV) and outer regions (508.56 ± 0.30 keV and 513.44 ± 0.30 keV), respectively. The S-parameter is a fraction of positrons annihilating with low momentum valence electrons and represents vacancy type defects and their concentration. The W-parameter approximates overlap of positron wavefunction with high momentum core electrons. [4]

PALS data acquisition and analysis

After in-situ DB-VEPAS, variable energy positron annihilation lifetime spectroscopy (PALS) measurements were conducted on two Si samples at the mono-energetic positron source (MePS) beamline at HZDR, Germany [5,6]. The MePS beamline is the end station of the radiation source ELBE, (Electron Linac for beams with high Brilliance and low Emittance) at HZDR (Germany) [1,2] featuring a digital lifetime $CrBr_3$ scintillator detector 51 mm diameter (2") and 25.4 mm length (1") coupled to a Hamamatsu R13089-100 PMT with a μ-metal shield and housed inside a solid Au casing with a homemade software employing a SPDevices ADQ14DC-2X with 14 bit vertical resolution and 2 GS/s horizontal resolution and with a time resolution function down to about 0.205 ns [7]. The resolution function required for spectrum analysis uses two Gaussian functions with distinct intensities depending on the positron implantation energy, E_p, and appropriate relative shifts. All spectra contained at least $1 \cdot 10^7$ counts.

A typical lifetime spectrum N(t) is described by $N(t)=\Sigma (1/\tau_i) I_i \exp(-t/\tau_i)$, where τ_i and I_i are the positron lifetime and intensity of the i-th component, respectively ($\Sigma I_i=1$). All the spectra were deconvoluted using the non-linearly least-squared based package PALSfit fitting software [8] into few discrete lifetime components, which directly evidence few different defect types (sizes) [see Figure 4 in the main text]. The corresponding relative intensities reflect to a large extend concentration of each defect type (size). In general, positron lifetime is directly proportional to defects size, i.e., the larger is the open volume, the lower is the probability and longer it takes for positrons to be annihilated with electrons [9,10,11]. Positron lifetimes and intensities were measured as a function of positron implantation energy, E_p, or mean implantation depth, $\langle z \rangle$.

References

1. Puska, M. J. and Nieminen, R. M. Theory of positrons in solids and on solid surfaces. Reviews of modern Physics, 66.3, 841 (1994)
2. Asoka-Kumar, P. and Lynn, K. G. Applied Physics Letters, 57, 1634 (1990).
3. Schultz, P.J. and Lynn, K. G. Reviews of Modern Physics 60.3, 701 (1988).

4. Clement, M., De Nijs, J.M.M., Balk, P., Schut, H. and Van Veen, A., Journal of Applied Physics 79, 9029 (1996).
5. Wagner, A., Anwand, W., Attallah, A.G., Dornberg, G., Elsayed, M., Enke, D., Hussein, A.E.M., Krause-Rehberg, R., Liedke, M.O., Potzger, K. and Trinh, T.T. Journal of Physics: Conference Series 791.1, 012004 (2017).
6. Wagner, A., Butterling, M., Liedke, M. O., Potzger, K., and Krause-Rehberg, R., AIP Conference Proceedings 1970.1, 040003 (2018).
7. Hirschmann, E., Butterling, M., Acosta, U.H., Liedke, M.O., Attallah, A.G., Petring, P., Görler, M., Krause-Rehberg, R. and Wagner, A., Journal of Instrumentation, 16.8, P08001 (2021).
8. Olsen, J. V., Kirkegaard, P., Pedersen, N. J., and Eldrup, M., Physica Status Solidi C 4.10, 4004 (2007).
9. R. Krause-Rehberg and H. S. Leipner, Positron Annihilation in Semiconductors: Defect Studies, (1999).
10. Tuomisto, F. and Makkonen, I., Reviews of Modern Physics 85(4), 1583 (2013).
11. Agarwal, S., Liedke, M.O., Jones, A.C.L., Reed, E., Kohnert, A.A., Uberuaga, B.P., Wang, Y.Q., Cooper, J., Kaoumi, D., Li, N. and Auguste, R., Science Advances 6.31, eaba8437 (2020).